UNSUPERVISED MULTISCALE CHANGE DETECTION IN MULTITEMPORAL SYNTHETIC APERTURE RADAR IMAGES

Turgay Celik

National University of Singapore, Singapore
email: chmcelik@nus.edu.sg

ABSTRACT

In this paper, an unsupervised change detection technique for synthetic aperture radar (SAR) images is proposed by conducting probabilistic Bayesian inferencing with expectation maximization-based parameter estimation to perform unsupervised thresholding over the data collected from the dual-tree complex wavelet transform (DT-CWT) subbands generated at the various scales. The proposed approach exploits a DT-CWT-based multiscale decomposition of the log-ratio image aimed at achieving different scales of representation of the change signal. Experimental results obtained on multitemporal SAR images acquired by the ERS-1, and JERS satellites confirm the effectiveness of the proposed approach.

1. INTRODUCTION

Automatic change detection of a given scene, based on a set of images acquired at different time instances, has been quickly becoming fairly instrumental to many image processing applications nowadays. Important applications of change detection include environmental surveillance, remote sensing, medical diagnosis and treatment, infrastructure monitoring, driver assistance systems, to name a few [1].

Remote sensing imagery generally requires certain corrections due to undesirable sensor characteristics and other disturbing effects before performing data analysis. Typical corrections include noise reduction, radiometric calibration (sensor calibration, atmospheric correction, solar correction and topographic correction) and geometric correction [2]. In this paper, without loosing any generality, we assume that the changes between two images are only caused from the physical changes in the geographical area, and all typical corrections mentioned previously have been applied on the images before applying the proposed change detection method.

Change detection methods could be categorized as either supervised or unsupervised according to the nature of data processing. The former is based on a supervised classification method, which requires the availability of a ground truth in order to derive a suitable training set for the learning process of classifiers. The latter approach, which is adopted in our work, performs change detection by making a direct comparison of two multi-spectral images considered without incorporating with relying on any additional information. Several unsupervised change detection techniques have been proposed in the literature [3]. Most of the methods are developed based on the so-called difference image. In [4], two automatic techniques based on the Bayes theory for the analysis of the difference image are proposed. One allows an automatic selection of the decision threshold for maximizing the overall change detection error under the assumption that the pixels of difference image are spatially independent. The other analyzes the difference image by considering the spatial contextual information included in the neighborhood of each pixel. This approach based on the Markov Random Fields (MRFs) exploits the context of inter-pixel class dependency. In [5], the observed multitemporal images are modeled as MRFs in order to search for an optimal image of changes by means of the maximum a posteriori (MAP) probability decision criterion and the simulated annealing (SA) energy minimization procedure. There are many other change detection methods using the same framework for synthetic aperture radar (SAR) images [6, 7]. However, these methods are applied to the raw data domain and suffer from the inference of speckle noise.

Recently, the transform-domain analysis is applied for conducting change detection for SAR images using discrete wavelet transform (DWT) [8] to remedy the problems caused by the speckle noise. They proposed DWT-based multiscale decomposition of the log-ratio image (obtained by the logarithm of the pixel ratio of two co-registered observations of the same scene) aimed at achieving different scales (levels) of representation of the difference image (logarithm of the pixel ratio is equivalent to the difference of logarithm of each pixel). Each scale is characterized by a tradeoff between speckle noise reduction and preservation of image details. The final change detection result is obtained according to an adaptive scale-driven fusion algorithm. The method achieves good results but has two major disadvantages: the selection of an appropriate detection threshold and the property of shift-variance of DWT.

In this paper, an automatic change detection method is proposed by analyzing log-ratio image of two SAR images acquired from the same area coverage, but at two different time instances. The two images are first scaled up by a factor of two in both dimensions in order to produce change detection result on the same spatial grid as that of the original images. The log-ratio image of two SAR images is then represented by exploiting the DT-CWT [9], as it possesses attractive properties for image processing, namely, shift invariance and more directional information, when compared with the DWT. Note that the DT-CWT is a form of DWT but generating complex-valued coefficients. It is implemented with a dual-tree of filter banks such that one tree independently generates the real part, while the other tree yields the imaginary part of complex coefficients. At each scale, the DT-CWT produces six directional subbands, oriented at $\pm 15^\circ, \pm 45^\circ$, and $\pm 75^\circ$, while the DWT produces only three directional subbands, oriented at 0°, 45°, and 90°.

The change detection problem is then tackled by employing the Bayesian inferencing on the magnitude of low-pass and high-pass subbands. To estimate the involved parameters and probability densities of the Bayesian framework, the expectation maximization (EM) algorithm [10] is exploited

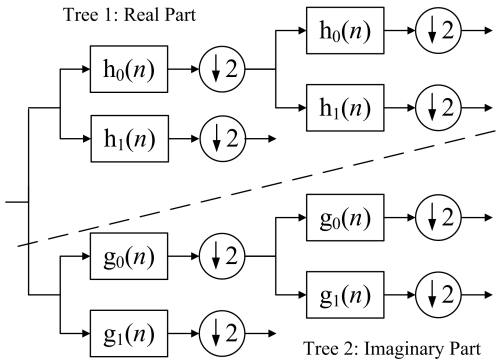

Figure 1: Two-level 1-D dual-tree complex wavelets transform (DT-CWT).

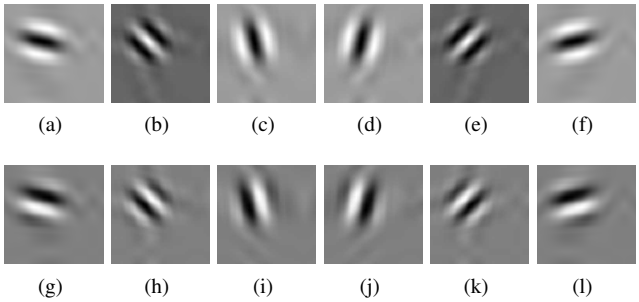

Figure 2: The real (R) and imaginary (I) parts of the impulse responses of the 2-D DT-CWT filters for the 6 directional subbands: (a) R_{-15°; (b) R_{-45°; (c) R_{-75°; (d) R_{+75°; (e) R_{+45°; (f) R_{+15°; (g) I_{-15°; (h) I_{-45°; (i) I_{-75°; (j) I_{+75°; (k) I_{+45°; (l) I_{+15°.

through iterations. Based on the final estimated densities, an unsupervised thresholding process can be established to determine whether it involves a change or no change at each pixel location. The binary mask of final change detection can be formed by eventually merging intra-scale and inter-scale information.

The paper is organized as follows. Section 2 gives a brief review of the DT-CWT. Section 3 describes the proposed multiscale change detection algorithm. Section 4 provides some experimental results of the proposed approach for both noise-free and noisy images. Section 5 concludes the paper.

2. COMPLEX WAVELETS

The ordinary DWT is not shift invariant because of the decimation operation exploited in the transform. A small shift in the input signal can cause a very different set of output wavelet coefficients. For that, Kingsbury [9] introduced a new kind of wavelet transform, called the dual-tree complex wavelet transform, that exhibits approximate shift invariant property and improved directional resolution with respect to DWT.

The DT-CWT also yields perfect reconstruction by using two parallel decimated trees with real coefficients. The one-dimensional (1-D) DT-CWT decomposes a signal $f(x)$ in terms of a complex shifted and dilated mother wavelet $\psi(x)$ and scaling function $\phi(x)$, i.e.,

$$f(x) = \sum_{l\in Z} s_{j_0,l}\phi_{j_0,l}(x) + \sum_{j\geq j_0}\sum_{l\in Z} c_{j,l}\psi_{j,l}(x), \qquad (1)$$

where j and l refer to the shifts and dilations respectively, $s_{j_0,l}$ is the scaling coefficient and $c_{j,l}$ is the complex wavelet coefficient with $\phi_{j_0,l}(x) = \phi^r_{j_0,l}(x) + \sqrt{-1}\phi^i_{j_0,l}(x)$, and $\psi_{j,l}(x) = \psi^r_{j,l}(x) + \sqrt{-1}\psi^i_{j,l}(x)$. The complex wavelet transform is a combination of two real wavelet transforms; in 1-D, the set $\{\phi^r_{j_0,l}, \phi^i_{j_0,l}, \psi^r_{j_0,l}, \psi^i_{j_0,l}\}$ forms a tight wavelet frame with two times of redundancy. The real and imaginary parts of the 1-D DT-CWT are computed using separate filter banks with wavelet filters h_0 and h_1 for the real part, and g_0 and g_1 for the imaginary part, as illustrated in Figure 1 [9]. The outputs from the two trees in Figure 1 are interpreted as the real and imaginary parts of the complex coefficients.

Similar to the 1-D DT-CWT, the two-dimensional (2-D) DT-CWT decomposes an 2-D image $f(x,y)$ through a series of dilations and translations of a complex scaling function and six complex wavelet functions ψ^θ, i.e.,

$$f(x,y) = \sum_{l\in Z^2} s_{j_0,l}\phi_{j_0,l}(x,y) + \sum_{b\in\theta}\sum_{j\geq j_0}\sum_{l\in Z^2} c^\theta_{j,l}\psi^\theta_{j,l}(x,y). \quad (2)$$

where $\theta = \{\pm 15^\circ, \pm 45^\circ, \pm 75^\circ\}$ refers to the directionality of the complex wavelet function. The impulse response of six complex wavelets associated with 2-D complex wavelet transform is illustrated in Figure 2. The complex wavelet transform can discriminate between features at positive and negative frequencies. Hence, there are six subbands capturing features along lines at angles of $\theta = \{\pm 15^\circ, \pm 45^\circ, \pm 75^\circ\}$.

3. CHANGE DETECTION ALGORITHM

3.1 Problem Formulation

Let us consider two SAR images, $\mathbf{X}_1 = \{x_1(i,j) \mid 1 \leq i \leq I, 1 \leq j \leq J\}$ and $\mathbf{X}_2 = \{x_2(i,j) \mid 1 \leq i \leq I, 1 \leq j \leq J\}$, with a size of $I \times J$ each acquired at the same geographical area but at two different time instances, t_1 and t_2, respectively. Let us further assume that such images have been registered with respect to each other [11,12] and that the possible differences due to the light and atmospheric conditions at the two time instances have been corrected [13]. Let $\Omega = \{w_c, w_u\}$ be the set of classes associated with changed (denoted by w_c) and unchanged (denoted by w_u) pixels on the images $\mathbf{X}_1$ and $\mathbf{X}_2$.

The decomposition of a 2-D signal by DT-CWT produces one complex-valued low-pass (approximation) subband and six complex-valued high-pass (detail) subbands at each level of decomposition. Let S-level decomposition of 2-D signal $\mathbf{X}$ of size $I \times J$ produces the complex-valued low-pass and high-pass subbands, and the magnitude of these subbands are denoted as $\mathbf{L}^{\mathbf{X}}_s = \{l^{\mathbf{X}}_s(i,j) \mid 1 \leq i \leq I/2^s, 1 \leq i \leq J/2^s\}$ and $\mathbf{H}^{\mathbf{X}}_{\theta,s} = \{h^{\mathbf{X}}_{\theta,s}(i,j) \mid 1 \leq i \leq I/2^s, 1 \leq i \leq J/2^s\}$, $\theta = \pm 15^\circ, \pm 45^\circ, \pm 75^\circ$ and $s = 1, \ldots, S$, respectively. That is, $\mathbf{L}^{\mathbf{X}}_s$ and $\mathbf{H}^{\mathbf{X}}_{\theta,s}$ are real-valued 2-D signal, representing the magnitude of complex-valued low-pass and high-pass subbands at a specific scale s, respectively.

3.2 Architecture of the Proposed Algorithm

The flowchart of the proposed multiscale change detection algorithm is given in Figure 3 and described as follows. Be-

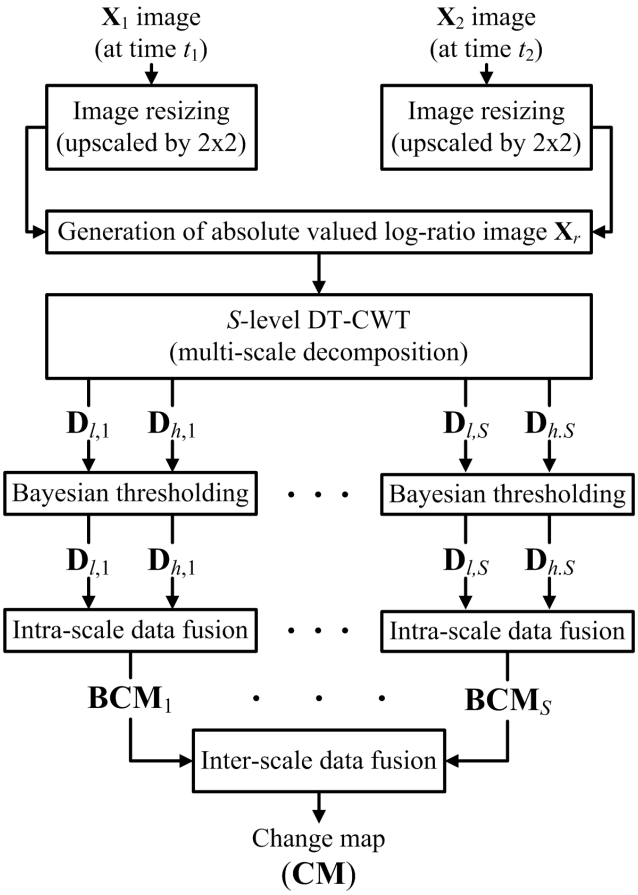

Figure 3: Proposed multiscale change detection algorithm.

cause of the decimation operation in DT-CWT decomposition, the size of subbands at the finest resolution (i.e., $S = 1$) is $I/2 \times J/2$. In order to create a change detection mask with the same size of that input images, firstly, the two input images, $\mathbf{X}_1$ and $\mathbf{X}_2$, are scaled up by a factor of 2 in both dimensions. To enhance low-intensity pixels, the ratio image is usually expressed in a logarithmic scale, resulting in the absolute valued log-ratio image $\mathbf{X}_r$

$$\mathbf{X}_r = \left| \log \frac{\mathbf{X}_1}{\mathbf{X}_2} \right| = |\log \mathbf{X}_1 - \log \mathbf{X}_2| \tag{3}$$

where log stands for natural-logarithm. $\mathbf{X}_r$ is decomposed by the DT-CWT up to scale S. At each scale s, $s = 1, 2, \ldots, S$, one complex-valued low-pass and six complex-valued high-pass subbands are generated, and the magnitude at each pixel of these subbands are computed and collectively denoted by $\mathbf{L}_s^{\mathbf{X}_r}$ and $\mathbf{H}_{\theta,s}^{\mathbf{X}_r}$, respectively, where $\theta \in \{\pm 15^\circ, \pm 45^\circ, \pm 75^\circ\}$. In order to detect changed pixels in high-pass subbands we define a new statistics which is the average of magnitudes of high-pass subbands, i.e.,

$$\mathbf{H}_s^{\mathbf{X}_r} = \frac{1}{6} \sum_{\forall \theta} \mathbf{H}_{\theta,s}^{\mathbf{X}_r}. \tag{4}$$

$\mathbf{L}_s^{\mathbf{X}_r}$ and $\mathbf{H}_s^{\mathbf{X}_r}$ can be viewed as 2-D random fields holding information on change pixels in low-pass and high-pass subbands at specific scale s, respectively. For the ease of mathematical notation, we represent $\mathbf{L}_s^{\mathbf{X}_r} = \mathbf{D}_{l,s} = \{d_{l,s}(i,j) \mid 1 \le i \le I/2^s, 1 \le i \le J/2^s\}$ and $\mathbf{H}_s^{\mathbf{X}_r} = \mathbf{D}_{h,s} = \{d_{h,s}(i,j) \mid 1 \le i \le I/2^s, 1 \le i \le J/2^s\}$. Unlike the classical unsupervised methods used in the remote sensing applications, Bayesian inferencing approach is proposed in this paper. Our final goal is to decide whether each pixel of $\mathbf{X}_2$ took at a later time instance is different from that of $\mathbf{X}_1$ acquired earlier; this binary decision process is conducted on the random fields $\mathbf{D}_{l,s}$ and $\mathbf{D}_{h,s}$. That is, the entire issue boils down to discriminating each coefficient of $\mathbf{D}_{l,s}$ and $\mathbf{D}_{h,s}$ into one of the two opposite classes, w_c or w_u, representing the involved pixel is changed or unchanged, respectively.

For this purpose the main problem to be solved is the estimation of a posterior probability density functions $p(d_{k,s}(i,j)|w_c)$ and $p(d_{k,s}(i,j)|w_u)$ and the a priori probabilities $P(w_c)$ and $P(w_u)$ of the classes w_c and w_u, respectively [4], where $k = \{l, h\}$. We assume that the probability density function $p(d_{k,s}(i,j))$ computed on the pixel values of the $\mathbf{D}_{k,s}$ can be modelled as a mixture density distribution consisting of two density distribution components, i.e.,

$$p(d_{k,s}(i,j)) = p(d_{k,s}(i,j)|w_c)P(w_c) + p(d_{k,s}(i,j)|w_u)P(w_u), \tag{5}$$

where $P(w_c) + P(w_u) = 1$. It is assumed that $p(d_{k,s}(i,j)|w_c)$ and $p(d_{k,s}(i,j)|w_u)$ can be modelled by the Gaussian distributions. In this manner, the density function associated with the class w_c can be described by the mean $\mu_{c,k,s}$ and the variance $\sigma^2_{c,k,s}$, and likewise the mean $\mu_{u,k,s}$ and the variance $\sigma^2_{u,k,s}$ for the class w_u. Now, the whole issue becomes how to estimate the values of these parameters and the above-mentioned a priori probabilities. In several problems, these terms are estimated by using supervised approaches that require the availability of a training set. In our work, an unsupervised approach is proposed instead, which exploits the expectation maximization (EM) algorithm [10], as follows.

The EM algorithm is a general approach used to conduct the maximum likelihood estimation for tackling incomplete-data problems, and it is an iterative process. In each iteration, it consists of two steps: expectation step and maximization step, which are iterated until the convergence is reached. The expectation step is computed with respect to the unknown underlying variables, using the current estimates of the parameters, and is conditioned by the observations [10]; that is,

$$v_{c,k,s}^{(t)}(i,j) = \frac{p^{(t)}\left(d_{k,s}(i,j)|w_c\right)}{p^{(t)}(d_{k,s}(i,j))} \tag{6}$$

$$P^{(t+1)}(w_c) = \frac{\sum_{i=1}^{I/2^s} \sum_{j=1}^{J/2^s} P^{(t)}(w_c)\, v_{c,k,s}^{(t)}(i,j)}{I/2^s \times J/2^s} \tag{7}$$

$$P^{(t+1)}(w_u) = 1 - P^{(t+1)}(w_c). \tag{8}$$

On the other hand, the maximization step provides new estimates of the parameters [10] for the distributions as

$$\mu_{c,k,s}^{(t+1)} = \frac{\sum_{i=1}^{I/2^s} \sum_{j=1}^{J/2^s} v_{c,k,s}^{(t)}(i,j)\, d_{k,s}(i,j)}{\sum_{i=1}^{I/2^s} \sum_{j=1}^{J/2^s} v_{c,k,s}^{(t)}(i,j)} \tag{9}$$

$$(\sigma^2_{c,k,s})^{(t+1)} = \frac{\sum_{i=1}^{I/2^s}\sum_{j=1}^{J/2^s} v^{(t)}_{c,k,s}(i,j)\ \left(d_{k,s}(i,j)-\mu^{(t)}_{c,k,s}\right)^2}{\sum_{i=1}^{I/2^s}\sum_{j=1}^{J/2^s} v^{(t)}_{c,k,s}(i,j)} \quad (10)$$

$$v^{(t)}_{u,k,s}(i,j) = \frac{p^{(t)}(d_{k,s}(i,j)|w_u)}{p^{(t)}(d_{k,s}(i,j))} \quad (11)$$

$$\mu^{(t+1)}_{u,k,s} = \frac{\sum_{i=1}^{I/2^s}\sum_{j=1}^{J/2^s} v^{(t)}_{u,k,s}(i,j)\ d_{k,s}(i,j)}{\sum_{i=1}^{I/2^s}\sum_{j=1}^{J/2^s} v^{(t)}_{u,k,s}(i,j)} \quad (12)$$

$$(\sigma^2_{u,k,s})^{(k+1)} = \frac{\sum_{i=1}^{I/2^s}\sum_{j=1}^{J/2^s} v^{(t)}_{u,k,s}(i,j)\ \left(d_{k,s}(i,j)-\mu^{(t)}_{u,k,s}\right)^2}{\sum_{i=1}^{I/2^s}\sum_{j=1}^{J/2^s} v^{(t)}_{u,k,s}(i,j)} \quad (13)$$

where the superscripts (t) and $(t+1)$ denote the iteration index.

After all parameters are estimated through iterations using (6) through (13), together with an assumption that the inter-pixels are independent, each pixel $d_{k,s}(i,j)$ will be assigned into one of the two classes: w_c or w_u. According to the Bayes rule, the minimization of the total decision error can be achieved by maximizing the conditional posteriori probability. Therefore, each pixel at the coordinate (i,j) is going to be labelled with one of the two classes, w_c and w_u, according to

$$\begin{aligned} C_{k,s}(i,j) &= \underset{w_i\in\{w_c,w_u\}}{\operatorname{argmax}} \left\{P\left(w_i|d_{k,s}(i,j)\right)\right\} \\ &= \underset{w_i\in\{w_c,w_u\}}{\operatorname{argmax}} \left\{\frac{P(w_i)\ p\left(d_{k,s}(i,j)|w_i\right)}{p\left(d_{k,s}(i,j)\right)}\right\}. \end{aligned} \quad (14)$$

Using (14), a binary image (or mask) $\mathbf{B}_{k,s} = \left\{b_{k,s}(i,j) \mid 1\le i\le I/2^s, 1\le j\le J/2^s\right\}$ can be created for each $k\in\{l,h\}$ at the scale s, in which '1' indicates that the corresponding pixel location involves a change, whereas '0' involving no changes. This process can be viewed as unsupervised thresholding according to

$$b_{k,s}(i,j) = \begin{cases} 1, & \frac{p\left(d_{k,s}(i,j)|w_c\right)}{p\left(d_{k,s}(i,j)|w_u\right)} \ge \frac{P(w_u)}{P(w_c)}; \\ 0, & \text{otherwise.} \end{cases} \quad (15)$$

Based on all $\mathbf{B}_{k,s}$, the total change mask, $\mathbf{BCM}_s$, at scale s is generated by performing intra-scale data fusion; i.e.,

$$\mathbf{BCM}_s = \mathbf{B}_{l,s} \mid \mathbf{B}_{h,s} \quad (16)$$

where $\mid$ performs binary union operations. In Figure 4, a set of two co-registered ERS-1 SAR images of a rice plantation in Java Island, Indonesia, $\mathbf{X}_1$ and $\mathbf{X}_2$, are used to demonstrate the performance of the change mask generation by the proposed algorithm at scale $s=1$ according to (15) and (16). The resultant change mask at $s=1$ shown in Figure 4 (f) is produced according to the (16) by combining change masks $\mathbf{B}_{l,1}$ and $\mathbf{B}_{h,1}$.

The same set of two input SAR images as shown in Figure 4 (a)-(b) are used to demonstrate the performance of the change detection generated by (16) at different scales, i.e., $s=1$ (Figure 5 (a)), $s=2$ (Figure 5 (b)), and $s=3$ (Figure 5 (c)). It is further noticed from Figs. 5 (a)-(c) that finer resolution tends to yield more false detections. This phenomenon can be effectively overcome by jointly considering all the binary change masks across all scales. The main reason for this is that any noticeable change should be detected in coarser resolution too. Based on this intuition, the final change mask can be generated by conducting the inter-scale data fusion; i.e.,

$$\mathbf{CM} = \bigcap_{s=1}^{S} \Phi(\mathbf{BCM}_s) \quad (17)$$

where S is the total number of scales used, $\bigcap$ performs binary AND operations, and $\Phi(\mathbf{BCM}_s)$ is an interpolation function which upscales $\mathbf{BCM}_s$ by a factor of 2^{s-1} in each dimension simply using nearest-neighbor interpolation. Figure 5 (d) shows the final merged change mask $\mathbf{CM}$ based on (17).

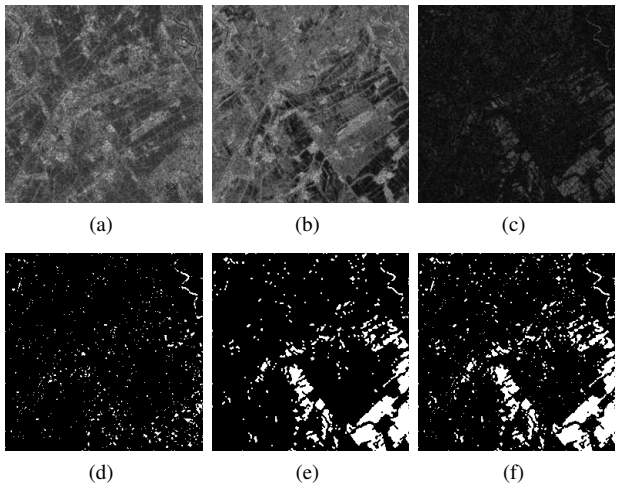

Figure 4: Change detection mask generation at scale $s=1$: (a) $\mathbf{X}_1$, (b) $\mathbf{X}_2$, (c) $\mathbf{X}_r$, (d) $\mathbf{B}_{h,1}$, (e) $\mathbf{B}_{l,1}$, and (f) $\mathbf{BCM}_1$.

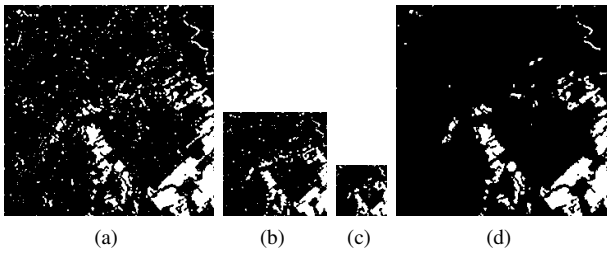

Figure 5: Change detection conducted in three scales and the resulted change masks for satellite images shown in Figure 4 (a)-(b): (a) change detection mask yielded at scale 1, $\mathbf{BCM}_1$, (b) change detection mask yielded at scale 2, $\mathbf{BCM}_2$, (c) change detection mask yielded at scale 3, $\mathbf{BCM}_3$, and (d) the change detection mask, $\mathbf{CM}$, resulted by merging all three binary masks according to (17).

4. EXPERIMENTAL RESULTS

We have applied the proposed method on different types of SAR images. Three scales (i.e., $S=3$) are used in DT-CWT

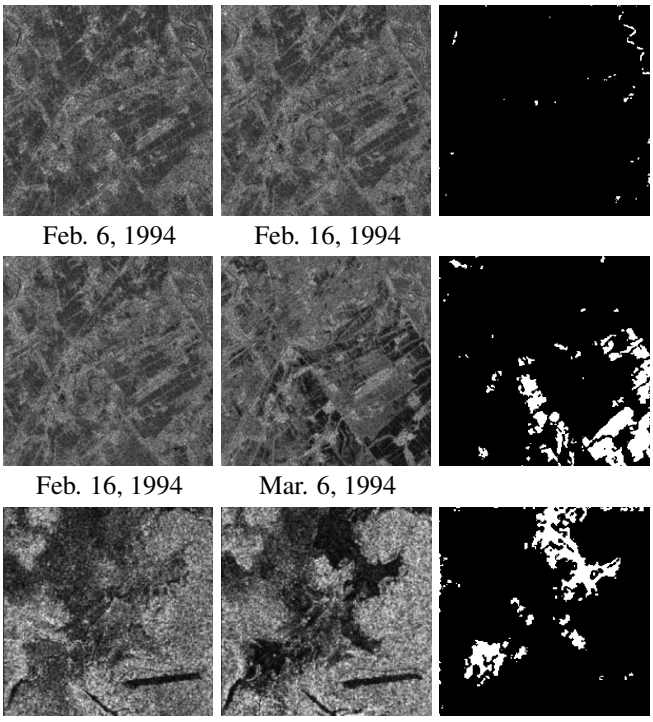

Figure 6: Change detection results using different sets SAR images, and the total number of scales $S = 3$: (a) Input image $\mathbf{X}_1$, (b) Input image $\mathbf{X}_2$, and (c) Final change detection masks, $\mathbf{CM}$.

decompositions. Columns (a) and (b) in Figure 6 display different sets of two satellite images which are used in our simulation as input samples. Column (c) of Figure 6 presents the final change mask for each experiment.

The input images shown in the first and second rows of Figure 6 are acquired from rice plantation in Semarang (Java Island) by ERS-1 [14]. The input images in the third row are JERS SAR channel 1 images of the airport at Cooinda, Kakadu National Park, Australia [15]. It is clear from Figure 6 column (c) that the resultant change masks accurately reflect the changes occured on the same geographical area taken at two different time instances.

5. CONCLUSION

An unsupervised change detection technique is developed by conducting probabilistic Bayesian inferencing with EM-based parameter estimation to perform unsupervised thresholding over the DT-CWT subbands generated at the various scales. At the each scale, the data in low-pass and high-pass subbands are processed separately to yield two different change masks, and those change masks are merged together to produce a single change mask. Since the proposed method only exploits spatial information, the resulted final change detection mask at each scale could yield higher false detection due to image noise. This drawback is overcome by exploiting the inter-scale information inherently provided by the DT-CWT to effectively reduce false detection rate.

REFERENCES

[1] R. Radke, S. Andra, O. Al-Kofahi, and B. Roysam, "Image change detection algorithms: a systematic survey," *IEEE Transactions on Image Processing*, vol. 14, no. 3, pp. 294–307, Mar 2005.

[2] M. Torma, P. Harma, and E. Jarvenpaa, "Change detection using spatial data problems and challenges," *IEEE International Geoscience and Remote Sensing Symposium (IGARSS 2007)*, pp. 1947–1950, Jul. 2007.

[3] P. Coppin, I. Jonckheere, and K. Nachaerts, "Digital change detection in ecosystem monitoring: A review," *International Journal of Remote Sensing*, vol. 25, no. 9, pp. 1565–1596, May 2004.

[4] L. Bruzzone and D. Prieto, "Automatic analysis of the difference image for unsupervised change detection," *IEEE Transactions on Geoscience and Remote Sensing*, vol. 38, no. 3, pp. 1171–1182, May 2000.

[5] T. Kasetkasem and P. Varshney, "An image change detection algorithm based on markov random field models," *IEEE Transactions on Geoscience and Remote Sensing*, vol. 40, no. 8, pp. 1815–1823, Aug. 2002.

[6] Y. Bazi, L. Bruzzone, and F. Melgani, "An unsupervised approach based on the generalized gaussian model to automatic change detection in multitemporal sar images," *IEEE Transactions on Geoscience and Remote Sensing*, vol. 43, no. 4, pp. 874–887, Apr 2005.

[7] P. Gamba, F. Dell'Acqua, and G. Lisini, "Change detection of multitemporal sar data in urban areas combining feature-based and pixel-based techniques," *IEEE Transactions on Geoscience and Remote Sensing*, vol. 44, no. 10, pp. 2820–2827, Oct 2006.

[8] F. Bovolo and L. Bruzzone, "A detail-preserving scale-driven approach to change detection in multitemporal sar images," *IEEE Transactions on Geoscience and Remote Sensing*, vol. 43, no. 12, pp. 2963–2972, Dec. 2005.

[9] B. Y. N. Kingsbury, "Image processing with complex wavelets," *Phil. Trans. Royal Society London A*, vol. 357, pp. 2543–2560, 1999.

[10] R. A. Redner and H. F. Walker, "Mixture densities, maximum likelihood and the em algorithm," *SIAM Review*, vol. 26, no. 2, pp. 195–239, Apr. 1984.

[11] J. Townshend, C. Justice, C. Gurney, and J. McManus, "The impact of misregistration on change detection," *IEEE Transactions on Geoscience and Remote Sensing*, vol. 30, no. 5, pp. 1054–1060, Sep. 1992.

[12] X. Dai and S. Khorram, "The effects of image misregistration on the accuracy of remotely sensed change detection," *IEEE Transactions on Geoscience and Remote Sensing*, vol. 36, no. 5, pp. 1566–1577, Sep. 1998.

[13] J. Chavez, P.S., "Radiometric calibration of landsat thematic mapper multispectral images," *Photogrammetric Engineering and Remote Sensing*, vol. 55, no. 9, pp. 1285–1294, 1989.

[14] S. Derrode, G. Mercier, and W. Pieczynski, "Unsupervised change detection in sar images using a multicomponent hmc model," in *MultiTemp*, 2003.

[15] http://ceos.cnes.fr:8100/cdrom-00b/ceos1/datapic/jers_sar/jerssar.htm#img. Accessed 9 February 2009.